Available online at www.sciencedirect.com
SCIENCE DIRECT®
Mechanics of Materials 38 (2006) 1090–1103
MECHANICS OF MATERIALS
www.elsevier.com/locate/mechmat

Flow stress of Nitronic-50 stainless steel over a wide range of strain rates and temperatures

Wei-Guo Guo [a], Sia Nemat-Nasser [b,*]

[a] School of Aeronautics, Northwestern Polytechnical University, Xi'an 710072, PR China
[b] Center of Excellence for Advanced Materials, Department of Mechanical and Aerospace Engineering, University of California, San Diego, 9500 Gilman Drive, La Jolla, CA 92093-0416, USA

Received 12 August 2005

Abstract

To understand and model the thermomechanical response of Nitronic-50 stainless steel, uniaxial compression tests are performed on cylindrical samples, using an Instron servohydraulic testing machine and an enhanced Hopkinson technique. True strains exceeding 60% are achieved in these tests, over the range of strain rates from 0.001/s to 8000/s, and at initial temperatures from 77 K to 1000 K. To understand the underlying deformation mechanisms, the microstructures of the undeformed and deformed samples are examined by optical microscopy.

These experimental results show that: (1) Nitronic-50 stainless steel displays good ductility (strain > 35%) for all considered strain rates, even at a 77 K temperature; (2) at high strain rates and 77 K initial temperature, adiabatic shearbands develop when the axial strain exceeds about 35%, leading to fracture; and (3) dynamic strain aging occurs at temperatures between 400 K and 1000 K for a strain rate of 0.001/s, but it is less pronounced at a strain rate of 3500/s or greater. Finally, based on the mechanism of dislocation motion and the experimental data, a physics-based model is developed for the deformation behavior of this material, including the effect of viscous drag on the motion of dislocations, but excluding the dynamic strain aging effects. The model predictions are compared with the results of the experiments. Good agreement between the theoretical predictions and experimental results is obtained.

Keywords: Nitronic-50; Strain rate; Temperature; Aging; Modeling

1. Introduction

Nitronic-50, also known as 22-13-5 stainless steel, is a weldable, nitrogen-strengthened austenitic stainless steel whose strength and corrosion resistance are superior to those of 304 and 316 stainless steels (see Denhard and Espy, 1972; Ritter and Henry, 1985; Ritter, 1988). The high chromium and molybdenum content of Nitronic-50 makes it superior to grades 316 and 316L in corrosion resistance in various environments, rivaling nickel alloys in seawater. For example, it was reported that, after exposure to 5% NaCl fog at 35 °C for 500 h, and after exposure to marine atmospheres 24 m from the high water line at KURE Beach, USA, for 7.5 years, no change was visible in Nitronic-50,

* Corresponding author. Tel.: +1 858 534 4914; fax: +1 858 534 2727.
E-mail address: sia@ucsd.edu (S. Nemat-Nasser).

0167-6636/$ - see front matter © 2006 Elsevier Ltd. All rights reserved.
doi:10.1016/j.mechmat.2006.01.004

while a similar exposure produces light staining on grade 316 stainless steel. And, unlike many austenitic stainless steels, Nitronic-50 does not become magnetic when cold worked or cooled to sub-zero temperatures. High strength (HS) Nitronic-50 stainless steel has a yield strength about three times that of type 316 stainless steel. Nitronic-50 stainless is readily arc welded in all forms. As with most austenitic stainless steels, good weld joint properties can be obtained without the necessity of preheat or post-weld annealing. Good shielding of the molten weld puddle is important to prevent any absorption of nitrogen from the atmosphere that could result in porosity. Nitronic-50 stainless steel is a structural steel, used in naval and other applications, including pumps, valves and fittings, fasteners, cables, chains, screens and wire cloth, marine hardware, boat and pump shafting, heat exchanger parts, springs and photographic equipment.

It is known that austenitic stainless steels exhibit a single-phase, face-centered cubic (fcc) structure that is maintained over a wide range of temperatures. This structure results from a balance of alloying additions that stabilize the austenite phase from elevated to cryogenic temperatures. Because these alloys are predominantly single phase, they can only be strengthened by solid-solution alloying or by work hardening. Several studies have addressed the strain-rate and temperature effects on the strength of austenitic stainless steels (see Hecker et al., 1982; Stout and Follansbee, 1986; Brooks and Lippold, 1990; Ishikawa and Tanimura, 1992). However, the plastic deformation of Nitronic-50 at low to high temperatures and over a wide range of strain rates, has received relatively little attention. The present paper addresses two major objectives. First, in order to examine the plastic flow of Nitronic-50 and the corresponding deformation mechanisms, systematic compression experiments are performed at low to high strain rates and over a wide range of temperatures, using the recovery techniques developed by Nemat-Nasser et al. (1991) and Nemat-Nasser and Isaacs (1996). Second, using the experimental data, the constitutive parameters of a model developed by Nemat-Nasser and Li (1998) and Nemat-Nasser et al. (2001) are calculated and the model predictions are compared with experimental results, including data that have not been used to evaluate the model parameters. This model is based on the mechanisms of thermally activated dislocation motion, and includes the drag-controlled effects and the effect of the elastic field of the forest of dislocations and other defects. The model, however, does not include the effect of the dynamic strain aging which is observed at low strain rates over the temperature range of 400–1000 K.

2. Experimental procedure and results

2.1. Material and samples

The nominal chemical composition of this commercial Nitronic-50 stainless steel is shown in Table 1.

The samples are cylindrical, 4 mm in diameter and height. To reduce the end friction during the experiments, the sample ends are first polished using waterproof silicon carbide paper, 1200 and 4000 grid, and then they are greased in the low- and room-temperature tests. A molybdenum-powder lubricant is used in the high-temperature experiments. It is known that the austenitic stainless steels exhibit good oxidation resistance at elevated temperatures up to nearly 900 K (Brooks and Lippold, 1990). Therefore, no special atmosphere is needed below this temperature. To examine the microstructure of the undeformed and deformed samples, the samples are sectioned along the loading direction, then polished and etched, as required by standard metallography. The etching reagent is Aqua regia: 15 ml HCI and 5 ml HNO_3. Fig. 1 shows the microstructure of an undeformed sample. The average grain size in this figure is about 21 μm. Twins are observed in this untested material, possibly due to pre-thermal-mechanical treatments.

2.2. Low and high strain-rate tests

Compression tests at a strain rate of 0.001/s are preformed using an Instron hydraulic testing machine, over a wide range of temperatures, from 77 K to 1000 K, with true strains exceeding 60%. Elevated temperatures are attained with a high-intensity quartz-lamp, radiant-heating furnace in an argon environment (in the present work, argon atmosphere is used for temperatures exceeding 800 K). The temperature is measured using a thermocouple arrangement. The temperature is maintained constant to

Table 1
Nominal chemistry of Nitronic-50 (%)

Cr	Ni	Mn	Mo	Si	N	Fe
22	12.5	5	2.25	1.0 max	0.3	Bal.

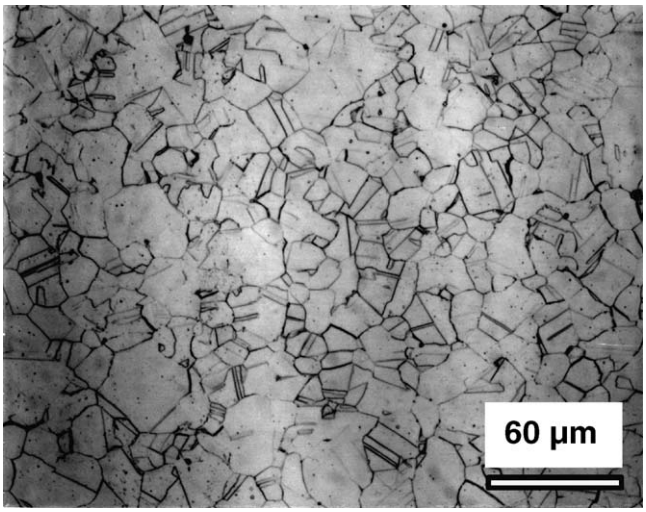

Fig. 1. Microstructure of Nitronic-50.

within ±2 °C. The deformation of the specimen is measured by LVDT, mounted in the testing machine, and is calibrated and compared with the results of a standard extensometer before each test. The low temperature of 77 K is obtained by immersing the specimen and the testing fixture in a bath of liquid nitrogen. The resulting true stress–true strain curves are displayed in Fig. 2.

Dynamic tests at a 3500/s strain rate and initial temperatures from 77 K to 1000 K are performed to strains exceeding 35%, using a recovery Hopkinson technique (Nemat-Nasser et al., 1991; Nemat-Nasser and Isaacs, 1996). For the high strain-rate tests at elevated temperatures, it is necessary to heat the sample to the required temperature while keeping the incident and transmission bars of the Hopkinson device at a suitably low temperature. To do this, Nemat-Nasser and Isaacs (1996) have developed a novel enhancement of the compression recovery Hopkinson technique (Nemat-Nasser et al., 1991), where a furnace is employed to preheat the specimen, while keeping the transmission and incident bars outside the furnace. These bars are then automatically brought into gentle contact with

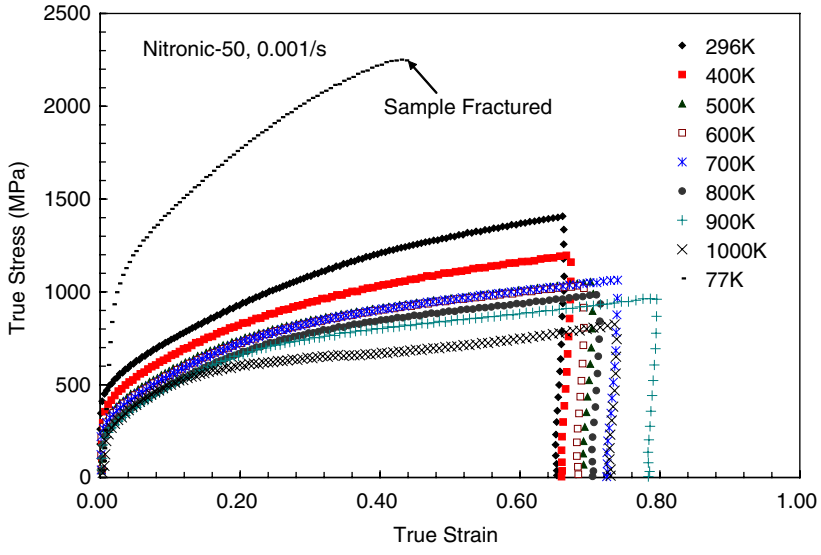

Fig. 2. True stress–true strain curves for the indicated temperatures and a strain rate of 0.001/s.

the specimen, just before the stress pulse reaches the specimen-end of the incident bar. The temperature is measured by a thermocouple which also holds the specimen inside the furnace. The true stress–true strain curves at a strain rate of 3500/s and indicated initial temperatures are shown in Fig. 3.

The recovery Hopkinson technique makes it possible to obtain the *isothermal flow stress at high strain rates and various temperatures*. The isothermal flow stress curves of Nitronic-50 at a strain rate of 3500/s and 77–500 K temperatures are given in Fig. 4, together with the corresponding adiabatic curves.

2.3. Discussion of experimental results

2.3.1. Nitronic-50's ductility

As is shown in Figs. 3 and 5, the samples that are tested at an initial temperature of 77 K, fracture at a strain of about 0.44 for a 0.001/s and at about 0.35 for a 3500/s strain rate. The sample tested at a strain rate of 3500/s displayed a visible shear failure. Fig. 5 shows the results of three tests at an initial temperature of 77 K and the indicated strain rates. Thus, at very low temperatures, the ductility of Nitronic-50 decreases with the increasing strain rate. This ductility improves at higher temperatures and low strain

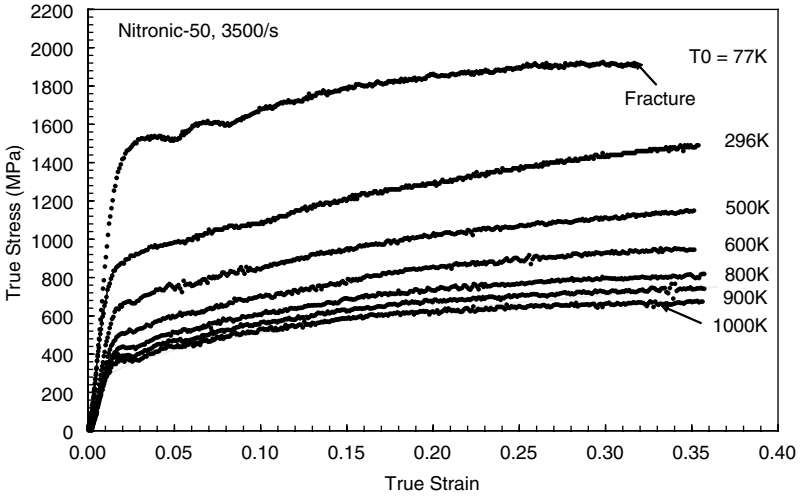

Fig. 3. Adiabatic stress–strain curves for indicated initial temperatures and a strain rate of 3500/s.

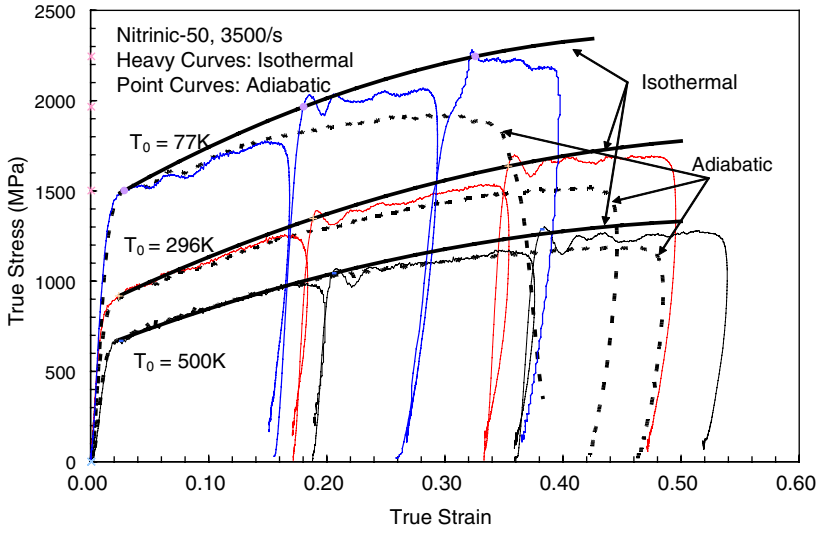

Fig. 4. Comparison between adiabatic and isothermal flow stress at 3500/s strain rate and indicated temperatures.

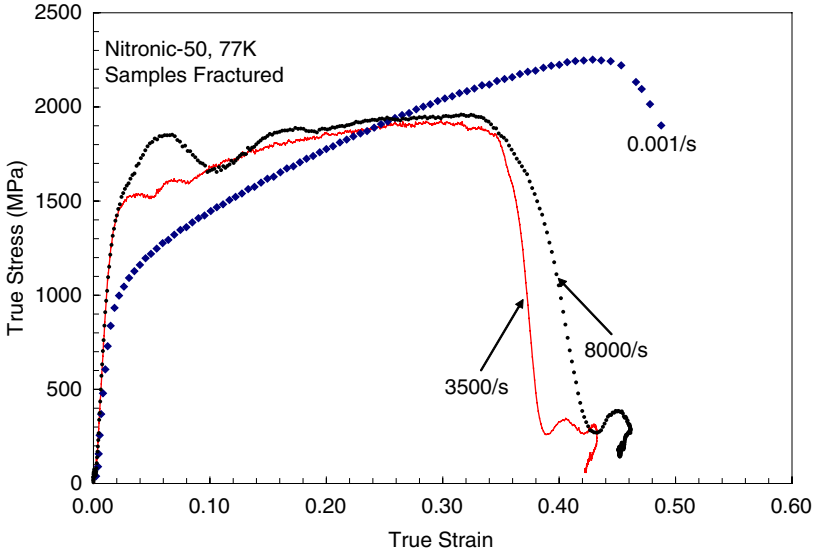

Fig. 5. True stress–true strain curves at 0.001/s, 3500/s, and 8000/s strain rates and 77 K initial temperature.

rates. For example, at a strain rate of 0.001/s and temperatures exceeding 296 K, the fracture strain can exceed 0.6.

2.3.2. Dynamic strain aging

The data in Figs. 2 and 3, suggest that the flow stress of Nitronic-50 is not very temperature-sensitive in the high-temperature range, where it may even increase with the increasing temperature, possibly due to dynamic strain aging. The term "static strain aging" (SSA) generally refers to the transient stress peaks observed in alloys with dilute solute atoms, when a prestrained specimen is totally or partially unloaded and aged for a prescribed time and then reloaded at the same prestraining strain rate. It is commonly accepted that this effect is related to the pinning of dislocations by diffusing solute atoms during the aging period. In general, dynamic strain aging is defined as recurrent pinning (serrated flow) of dislocations while arrested at obstacles during their motion that results in plastic straining (Kubin et al., 1992). Dynamic strain aging is generally attributed to the additional resistance to dislocation motion produced by the solute atoms that can diffuse to dislocations above a certain temperature (Beukel and Kocks, 1982) while the dislocations are "waiting" at their short-range barriers. During this waiting period, a Cottrell atmosphere and/or a core atmosphere can form at dislocations, depending on the temperature and strain rate (Nakada and Keh, 1970). In steel, the occurrence of static and dynamic strain aging results from the diffusion of C and N in the temperature range of 150–300 °C. Cho et al. (2000) report that the substitutional elements, Cr and Ni in 304 stainless steel, produce static strain aging at temperatures of 900–1100 °C.

In order to investigate the temperature sensitivity of this material, the stress–strain curves of Figs. 2 and 3 are reported in Figs. 6 and 7 as stress vs. temperature for the indicated strains and strain rates. As is seen in Fig. 6, when, at a strain rate of 10^{-3}/s, the test temperature is increased from 77 K to 400 K, the flow stress decreases, but as the temperature is further increased, the flow stress remains almost the same or it actually increases in the temperature range from 400 to 1000 K, attaining a peak value at about 700 K. This suggests that, solute atoms interact with the moving dislocations in this temperature range, retarding their motion.

With the increasing strain rate, higher temperatures are required to drive the solutes to the dislocations at sufficient speeds. As the solute atoms catch up with the moving dislocations and pin them down, the flow stress increases. In Fig. 7, for a strain rate of about 3500/s, the peak in the flow stress now occurs at about 800 K, showing the effect of higher strain rate; compare Figs. 6 and 7.

2.3.3. Strain-rate effect on flow stress

It is known that the flow stress of most materials increases with the increasing strain rate. In Fig. 8,

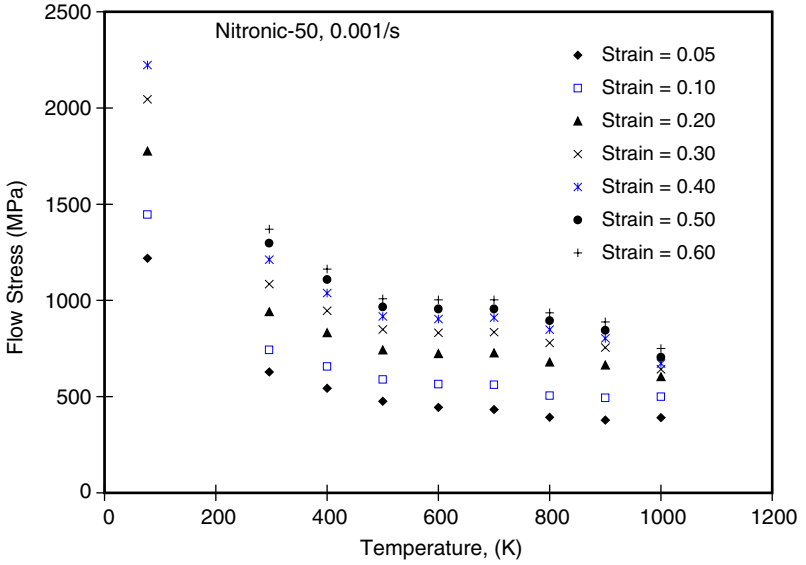

Fig. 6. Flow stress as a function of temperature for indicated strains at 0.001/s strain rate.

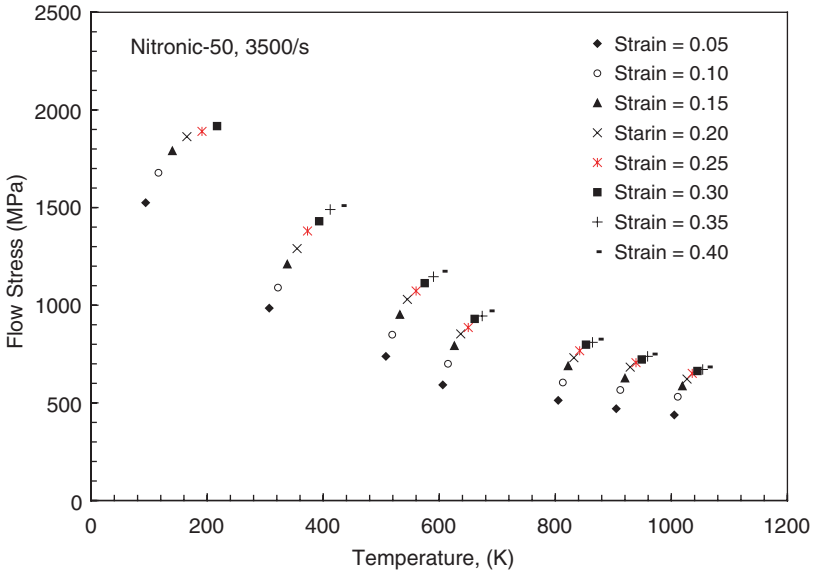

Fig. 7. Flow stress as a function of temperature for indicated strains at 3500/s strain rate.

the stress–temperature curves at various indicated strain rates are compared for a fixed strain of 20%. As is seen, the flow stress strongly depends on the strain rate, especially when the temperature exceeds 600 K and the dynamic strain-aging range shifts to the higher temperatures with the increasing strain rate. It is notable that the flow stress does not seem to be sensitive to the strain rate for temperatures exceeding 900 K. Fig. 9 shows the Nitronic-50's isothermal flow stress vs. the strain rate, at indicated temperatures; the curve for the 3500/s strain rate is obtained using the data given in Fig. 4. As is seen in Fig. 9, the stress increases with the increasing strain rate, especially when the strain rate exceeds about 1000/s. This increased strain-rate sensitivity is usually attributed to the additional drag forces that are developed at higher strain rates, and which further retard the mobile dislocations (see Follansbee and Weertman, 1982; Regazzoni et al., 1987; Chiem, 1992; Zerilli and Armstrong, 1992).

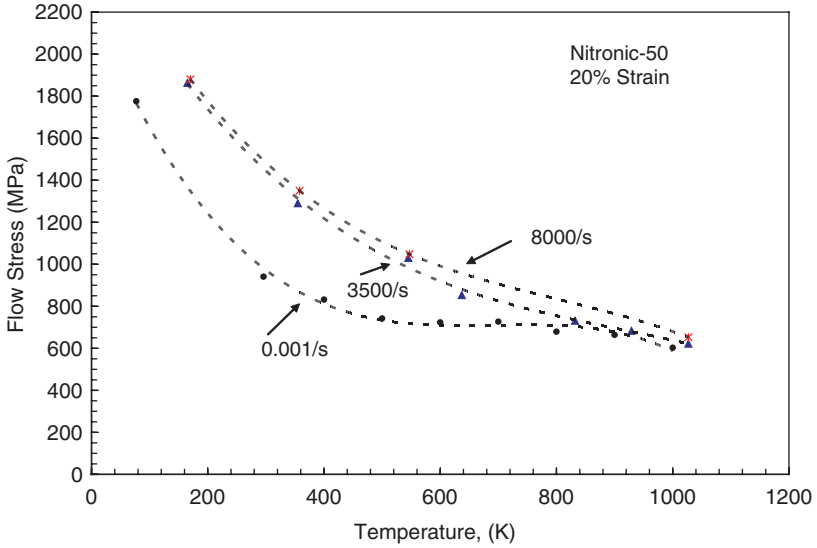

Fig. 8. Effect of strain rates on flow stress at a true strain of 10%.

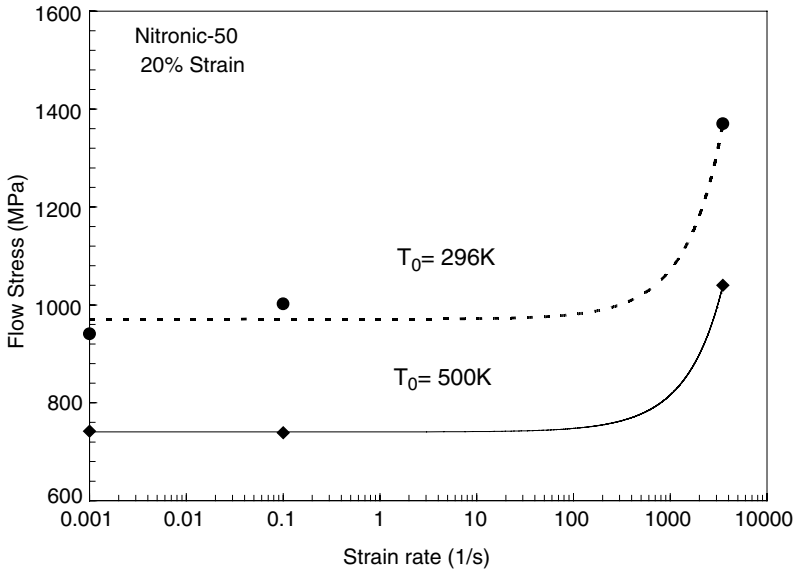

Fig. 9. Flow stress as a function of strain rate at 20% strain.

3. Physically based constitutive model

3.1. Evaluation of plastic work–heat conversion factor

Plastic deformation generates heat, which is either dissipated to the surroundings or used to increase the temperature of the material. When the rate of heat generation exceeds that of heat loss, the temperature of the material increases. This generally happens at high strain rates. For materials whose flow stress is temperature dependent, a continuous rise in temperature during deformation results in simultaneous lowering of the flow stress. The temperature rise of a sample can be calculated from

$$\Delta T = \int_0^{\gamma} \frac{\beta}{\rho' C_V} \tau \, \mathrm{d}\gamma, \tag{3.1}$$

where ρ' is the mass density (7.8 g/cc), C_V is the temperature-dependent heat capacity (taken as

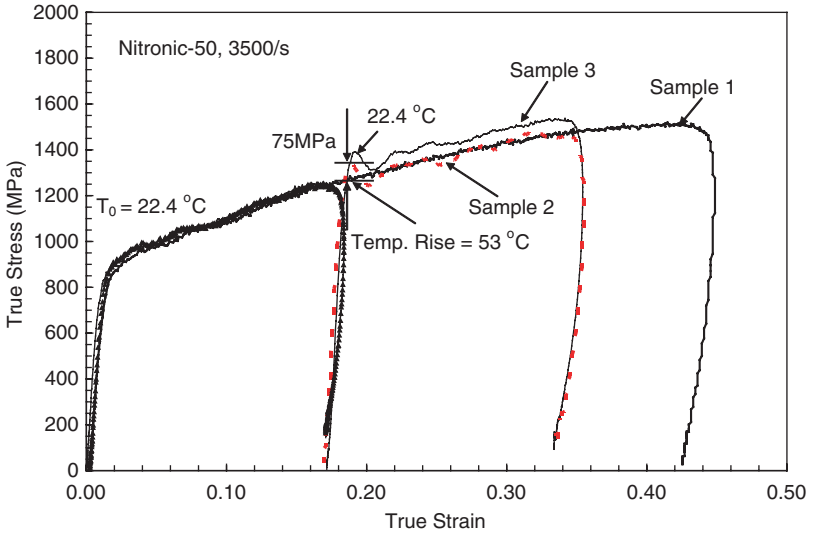

Fig. 10. Verification of heat conversion.

0.5 J/g K at room temperature), γ is the plastic strain, τ is the flow stress in MPa, and β is the fraction of the plastic work which is converted into heat. The value of β is determined experimentally. Data reported by Kapoor and Nemat-Nasser (1998) for several metals suggest that, for large strains (e.g., $\gamma \geqslant 20\%$), β is essentially 1. This has also been verified to be the case for several other polycrystalline metals (see Nemat-Nasser et al., 1999, 2001). In the present case, we have also found that $\beta \approx 1.0$ for strains exceeding 10–20%.

To examine whether or not $\beta \approx 1.0$ for Nitronic-50 steel, an indirect experiment is performed. The area under the true stress–true strain curve gives the plastic work per unit volume in uniaxial deformation. In Fig. 10, three samples (designated as 1, 2, and 3, respectively) are loaded at the same strain rate of 3500/s. Sample 1 is loaded to a true strain of about 43% at an initial temperature of 22.4 °C (room temperature). The corresponding true stress–true strain curve is displayed by a thick curve in Fig. 10. This is essentially an adiabatic true stress–true strain relation for Nitronic-50 at a 3500/s strain rate. The temperature rise in this adiabatic test is calculated using Eq. (3.1), assuming $\beta \approx 1.0$.

Samples 2 and 3 are first loaded to a true strain of 18%, starting at room temperature (22.4 °C). Their true stress–true strain relations are shown by thick solid curves in Fig. 10. These curves fall on the curve corresponding to sample 1, showing the reproducibility of the test results. The temperature rise at a true strain of 18% is 53 °C, calculated by Eq. (3.1) with $\beta \approx 1.0$. Then sample 2 is heated to 75.4 °C (53 + 22.4) that corresponds to the initial temperature of 22.4 °C, and is reloaded at the same strain rate, producing the second dotted curve, shown in Fig. 10. This curve follows closely the adiabatic curve of sample 1. As a further check, sample 3 is reloaded at its initial room temperature (22.4 °C), and the corresponding true stress–true strain curve is displayed by the thin solid curve marked sample 3. The stress difference between the adiabatic curve and this isothermal curve is measured to be about 75 MPa, for a strain increment of 18%. It is clear that this stress difference (75 MPa) is due to thermal softening of the material. Two important conclusions are drawn from these results: (1) if there was any recovery between unloading and reloading, it did not affect the flow stress noticeably, as the interrupted curve of sample 2 follows the uninterrupted curve of sample 1; and (2) essentially the entire plastic work is converted to heat with a negligibly small amount being stored in the sample as the elastic energy of the dislocations and other defects, or lost through sample boundaries.

3.2. Phsically based constitutive model

The experimental results reveal the following characteristics for Nitronic-50 stainless steel: (1) the plastic flow stress of this material is both temperature- and strain rate-dependent; (2) the dynamic strain aging occurs at low strain rates in the temperature range of 400–1000 K (Fig. 6), becoming

weaker with increasing strain rates, or when the temperature exceeds 1000 K, but increasing with strain and attaining a peak value at about 700 K; and (3) there is a viscous-drag resistance to the motion of dislocations, at high strain rates (Fig. 9).

A suitable constitutive model for this material should therefore include all the above effects. Based on the concept of dislocation kinetics, paralleled with a systematic experimental investigation, a physically based model is developed by Nemat-Nasser and Isaacs (1996) and Nemat-Nasser and Li (1998) for several polycrystalline metals. A similar model which includes all the characteristics observed in Nitronic-50 stainless steel does not currently exist. In the present work, we seek to incorporate the experimental data presented above for Nitronic-50, into the constitutive model suggested by Nemat-Nasser and co-workers; see Nemat-Nasser (2004) for a comprehensive account. In what follows, we will not seek to include the dynamic strain aging effects in the model.

We consider the plastic flow in the range of temperatures and strain rates where diffusion and creep are not dominant, and the deformation occurs basically by the motion of dislocations. We assume that the flow stress can be expressed as a combination of the thermal and athermal parts of the resistance to the dislocation motion. Here, for the Nitronic-50 alloy, we assume that the flow stress, τ, consists of three parts: One part essentially due to the short-range thermally activated effect which may include the Peierls stress, point defects such as vacancies and self-interstitials, other dislocations which intersect the slip plane, alloying elements and solute atoms (interstitial and substitutional). We denote this by τ^*. The second part is the athermal component, τ_a, mainly due to the long-range effects such as the stress field of dislocation forests and grain boundaries. Finally, a remaining viscous-drag component, τ_d, which usually is important at high-temperatures and high strain rates. Thus, the flow stress is written as,

$$\tau = \tau_a + \tau_d + \tau^*. \tag{3.2}$$

In this formulation, the total flow stress of the material, τ, is assumed to be a function of the strain rate, $\dot{\gamma}$, temperature, T, and some internal parameters that reflect the material's microstructure, i.e., the average grain size, the distribution of second phase particles or precipitates, and the distribution and density of the dislocations. In general, the most commonly used microstructural parameter is the average dislocation density, ρ. The microstructure can evolve differently for different loading conditions, that is, for different current values and histories of $\dot{\gamma}$ and T.

3.2.1. Athermal stress component, τ_a

The athermal part, τ_a, of the flow stress, τ, is independent of the strain rate, $\dot{\gamma}$. The temperature effect on τ_a is only through the temperature dependence of the elastic modulus, especially the shear modulus, $\mu(T)$ (Conrad, 1970). τ_a mainly depends on the microstructure of the material, e.g., the dislocation density, grain sizes, point defects, and various solute atoms such as those listed in Table 1. Based on linear elasticity, τ_a would be proportional to $\mu(T)$. Hence, we may set

$$\tau_a = f(\rho, d_G, \ldots)\mu(T)/\mu_0, \tag{3.3}$$

where ρ is the average dislocation density, d_G is the average grain size, the dots stand for parameters associated with other impurities, and μ_0 is a reference value of the shear modulus. In a general loading, the strain γ represents the effective plastic strain which is a monotonically increasing quantity in plastic deformation. In the present case, γ defines the loading path and is also a monotonically increasing quantity since $\dot{\gamma} > 0$. Therefore, it can be used as a load parameter to define the variation of the dislocation density, the average grain size, and other parameters which affect τ_a, i.e., we may set

$$\begin{aligned}\tau_a &= f(\rho(\gamma), d_G(\gamma), \ldots)\mu(T)/\mu_0 \\ &= \hat{f}(\gamma)\mu(T)/\mu_0.\end{aligned} \tag{3.4}$$

Further, as a first approximation, we may use a simple power-law representation of $\hat{f}(\gamma)$, and choose an average value for μ_0 so that $\mu(T)/\mu_0 \approx 1$. Then, τ_a may be written as

$$\tau_a \approx a_0 + a_1\gamma^n + \cdots, \tag{3.5}$$

where a_0, a_1, and n are free parameters which must be fixed experimentally.

3.2.2. Viscous-drag component, τ_d

The viscous-drag stress, τ_d, may be related to the dislocation motion by assuming that $\tau_d \approx MBv/b$, where M is the Taylor factor, B is the drag coefficient, v is the average dislocation velocity, and b is the magnitude of the Burgers vector. Since v relates to the strain rate by $\dot{\gamma} = \rho_m bv/M$ (where ρ_m is the mobile dislocation density), it follows that $\tau_d \approx g(M^2B/(\rho_m b^2), \dot{\gamma}, T)$. At high temperatures, and in

the absence of creep and dynamic strain aging, the flow stress is essentially independent of the temperature, T, and we may assume

$$\tau_d \approx g(M^2B/(\rho_m b^2), \dot{\gamma}). \tag{3.6}$$

To examine the effect of the viscous drag on the flow stress of this Nitronic-50, we set

$$\tau_d = m_0[1 - \exp(-\alpha\dot{\gamma})], \qquad \alpha = \frac{M^2B}{\rho_m b^2 \tau_{0.2}}, \tag{3.7}$$

where m_0 is a material constant which can be measured directly at a very high strain rate, and α represents an effective damping coefficient affecting the dislocation motion. For the present metal, we take the Taylor factor as $M \approx 2.75$, $b \approx 3\times10^{-10}$ m, $B = 5\times10^{-3}$ Pa s, and $\rho_m = O(10^{13}\ m^{-2})$. $\tau_{0.2}$ is the reference yield stress which is assumed to be independent of the temperature. In our experiments, a value of about 140 MPa is obtained for m_0 from the trend of the flow stress at a 1000 K temperature and a strain rate of 0.1/s. Thus, with $\alpha \approx 3\times10^{-4}$ and $m_0 \approx 140$ MPa, the viscous-drag component of the flow stress becomes

$$\tau_d = 140[1 - \exp(-3\times10^{-4}\dot{\gamma}). \tag{3.8}$$

3.2.3. Athermal- and drag-stress components of Nitronic-50

To identify the constitutive parameters for the athermal stress in Eq. (3.4), we examine the variation of the flow stress with temperature, as shown in Figs. 6–8. These results suggest that the flow stress becomes essentially independent of the temperature, close to 1000 K and greater temperatures. The following final expression for the athermal and drag components of the flow stress is obtained:

$$\tau_a + \tau_d = 940\gamma^{0.35} + 140[1 - \exp(-3\times10^{-4}\dot{\gamma})]. \tag{3.9}$$

3.2.4. Thermally activated component of the flow stress, τ^*

The thermally activated flow stress, τ^*, in general, is a function of temperature, T, strain rate, $\dot{\gamma}$, and the internal variables characterizing the microstructure of the material. Consider the average dislocation density, ρ, as the most dominant microstructural parameter. Its evolution may be related to the (monotonically increasing) effective plastic strain, γ; since $\dot{\gamma} > 0$, γ may be used as the loading parameter.

To obtain a relation between $\dot{\gamma}$, T, and τ^*, let ΔG be the activation free energy that a dislocation must overcome by its thermal energy. Kocks et al. (1975) suggest the following relation between ΔG and τ^*, representing a typical barrier encountered by a dislocation:

$$\Delta G = G_0\left[1 - \left(\frac{\tau^*}{\hat{\tau}}\right)^p\right]^q, \qquad G_0 = \hat{\tau}b\lambda\ell, \tag{3.10}$$

where $0 < p \leqslant 1$ and $0 \leqslant q \leqslant 1$ define the profile of the short-range barrier to the dislocation (Kocks et al., 1975; Ono, 1968), $\hat{\tau}$ is the shear stress above which the barrier is crossed by a dislocation without any assistance from thermal activation, and G_0 is the free energy required for a dislocation to overcome the barrier solely by its thermal activation; λ and ℓ are the average effective barrier width and the dislocation spacing, respectively. Based on an energy minimization, it can be shown (Nemat-Nasser, 2004) that $\dot{\gamma}$ can be related to ΔG by

$$\dot{\gamma} = \dot{\gamma}_r \exp\left\{-\frac{\Delta G}{kT}\right\}, \tag{3.11}$$

where $\dot{\gamma}_r = \rho_m b\bar{v}$; here ρ_m is the mobile dislocation density, k is the Boltzmann constant, and $\bar{v} = \omega_0\ell$ is the average velocity of the mobile dislocations, where ω_0 is the attempt frequency and ℓ is the average distance between barriers. From Eqs. (3.10) and (3.11), we now obtain

$$\tau^* = \hat{\tau}\left[1 - \left(-\frac{kT}{G_0}\ln\frac{\dot{\gamma}}{\dot{\gamma}_r}\right)^{1/q}\right]^{1/p}. \tag{3.12}$$

To account for the microstructural evolution which affects the average dislocation spacing, ℓ, Nemat-Nasser and Li (1998) have suggested the expression $\ell = \ell_0 f(\gamma, T)$ for the variation of ℓ with temperature, where ℓ_0 is a reference (e.g., initial) average dislocation spacing. In view of (3.10)–(3.12), this gives

$$\hat{\tau} = \tau^0 f(\gamma, T) \quad \text{and} \quad \dot{\gamma}_r = \frac{\dot{\gamma}_0}{f(\gamma, T)}, \qquad \tau^0 = \frac{G_0}{b\lambda\ell_0}, \quad \dot{\gamma}_0 = \rho_m b\omega_0\ell_0. \tag{3.13}$$

It is reasonable to expect that the average dislocation density increases with straining (work-hardening) and that it decreases with increasing temperature (annealing). Based on this observation, and guided by our experimental results, we follow Nemat-Nasser and Li and set,

$$f(\gamma,T)=\frac{\ell_0}{\ell}=1+a\left[1-\left(\frac{T}{T_{\mathrm{m}}}\right)^2\right]\gamma^m, \tag{3.14}$$

where ℓ_0 is a free parameter which depends on the initial average dislocation (the higher the initial dislocation density, the smaller is a), T_{m} is the melting temperature (approximately 1673 K for steels), and the index m is a free parameter which must be evaluated from the experimental data. Combining Eqs. (3.12) and (3.14), we arrive at the following expression for τ^*:

$$\begin{aligned}
&\tau^*=\tau^0\left\{1-\left[-\frac{kT}{G_0}\ln\frac{\dot\gamma f(\gamma,T)}{\dot\gamma_0}\right]^{1/q}\right\}^{1/p} f(\gamma,T)\\
&\quad\text{for } T\leqslant T_{\mathrm{c}},\\
&\tau^0=\frac{G_0}{b\lambda\ell_0},\quad \dot\gamma_0=b\rho_{\mathrm{m}}\omega_0\ell_0,\\
&f(\gamma,T)=\frac{\ell_0}{\ell}=1+a\left[1-\left(\frac{T}{T_{\mathrm{m}}}\right)^2\right]\gamma^m,
\end{aligned} \tag{3.15}$$

where T_{c} is given by

$$T_{\mathrm{c}}=-\frac{G_0}{k}\left(\ln\frac{\dot\gamma f(\gamma,T_{\mathrm{c}})}{\dot\gamma_0}\right)^{-1}. \tag{3.16}$$

Note that $\tau^*=0$ for $T>T_{\mathrm{c}}$.

In Eq. (3.15), the parameters p and q define the profile of the short-range energy barrier to the motion of dislocations. Ono (1968) and Kocks et al. (1975) suggest that $p=2/3$ and $q=2$ are suitable values for these parameters for many metals. Here, for Nitronic-50, we use these values for p and q in (3.15). The parameters k/G_0 and $\dot\gamma_0$ define the temperature and strain-rate dependency of the material. Greater temperature sensitivity is associated with larger k/G_0, whereas larger $\dot\gamma_0$ corresponds to a smaller strain-rate sensitivity. The product $(k/G_0)/\ln\dot\gamma_0$ can be estimated directly from the experimental data of Fig. 7. We have found that $k/G_0\approx 6.6\times10^{-5}\,\mathrm{K}^{-1}$ and $\dot\gamma_0\approx 2\times10^{10}/\mathrm{s}$ are suitable values in the present case. The first corresponds to an energy barrier of about 2 eV, and the second can be estimated by setting $b\approx 3\times10^{-8}$ cm, $\omega_0=\mathrm{O}(10^{12}/\mathrm{s})$, $\rho_{\mathrm{m}}=\mathrm{O}(10^{13}\,\mathrm{cm}^{-2})$, and ℓ_0 of about 5000 lattice spacing. For the other parameters, we choose $m=1/2$ which relates to the dislocation density, and set $a=5$. Finally, we fix τ^0 empirically at $\tau^0=800$ MPa which also has the correct order-of-magnitude, based on $\tau^0=G_0/(b\lambda\ell_0)$.

Now, the final constitutive relation for this material becomes, for $T\leqslant T_{\mathrm{c}}$,

$$\begin{aligned}
\tau&=940\gamma^{0.35}+140[1-\exp(-3\times10^{-4}\dot\gamma)]\\
&\quad+800\left\{1-\left[-6.6\times10^{-5}T\ln\frac{\dot\gamma f(\gamma,T)}{2\times10^{10}}\right]^{1/q}\right\}^{1/p} f(\gamma,T),
\end{aligned} \tag{3.17}$$

where

$$\begin{aligned}
T&=T_0+0.25\int_0^\gamma \tau\,\mathrm{d}\gamma,\quad f(\gamma,T)\\
&=1+5\left[1-\left(\frac{T}{1673}\right)^2\right]\gamma^{1/2}
\end{aligned}$$

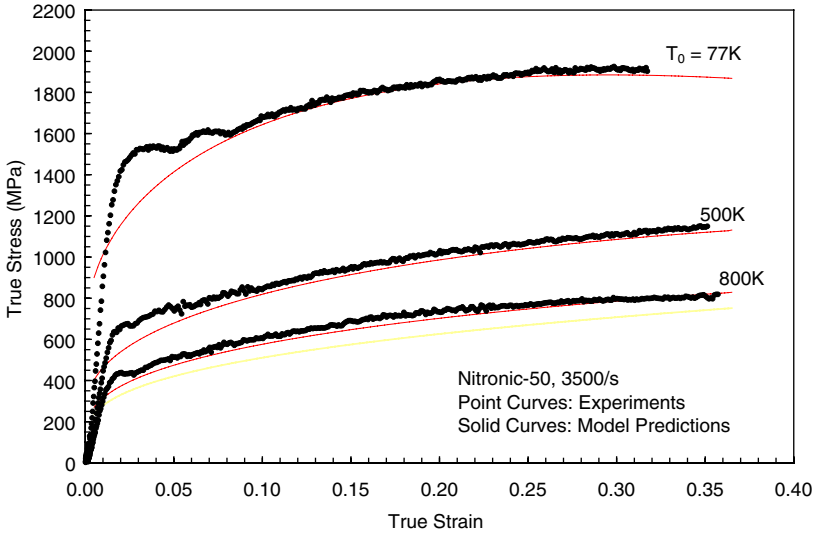

Fig. 11. Comparison of model predictions with experimental results at a strain rate of 3500/s.

and for $T > T_c$,

$$\tau = 940\gamma^{0.35} + 140[1 - \exp(-3 \times 10^{-4}\dot{\gamma})], \qquad (3.18)$$

where

$$T_c = \left[-6.6 \times 10^{-5} \ln \frac{\dot{\gamma} f(\gamma, T_c)}{2 \times 10^{10}}\right]^{-1}.$$

Figs. 11–13 compare the experimental results with the model predictions at the strain rates of 3500/s and 8000/s, for the indicated initial temperatures. As is seen, good correlation between these data and the model predictions is obtained.

As pointed out before, the model does not include the dynamic strain aging effects, which occur in the temperature range of 400–1000 K, at low strain rates of 0.001/s and 0.1/s. In Figs. 14 and 15 compare the experimental results with the model predictions at a fixed temperature of 296 K. Aside from the effect of dynamic strain aging, the model predictions are basically in reasonable agreement with the experimental results.

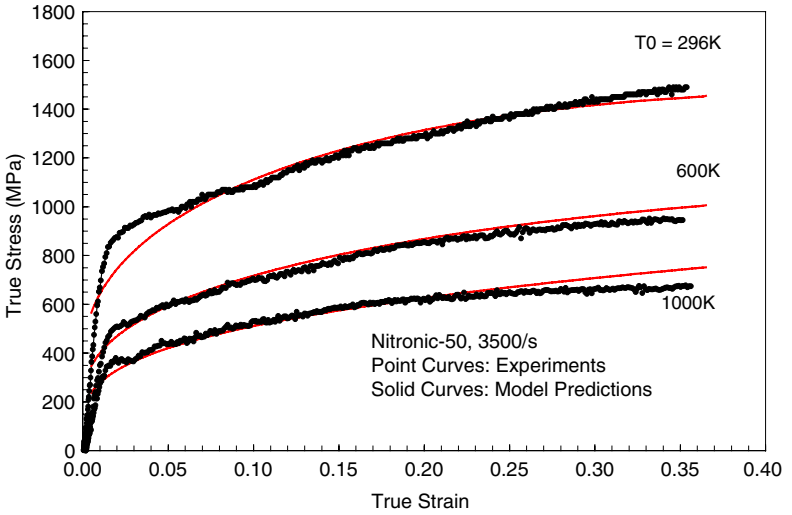

Fig. 12. Comparison of model predictions with experimental results at a strain rate of 3500/s.

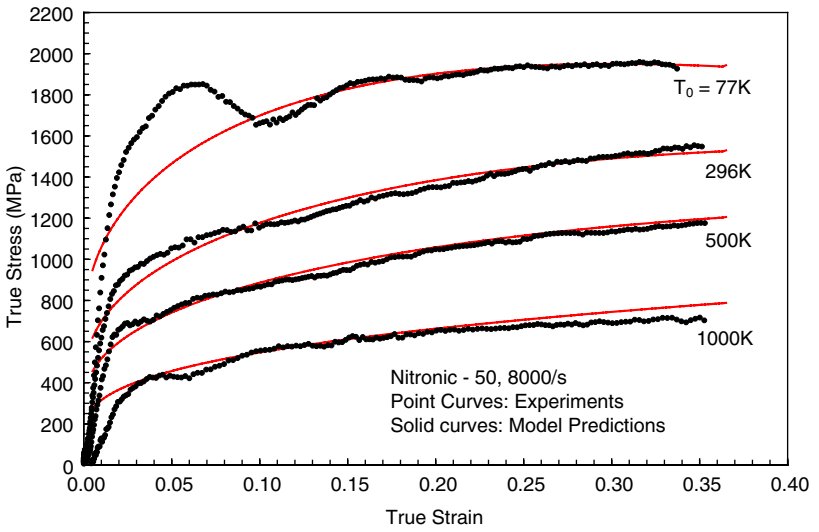

Fig. 13. Comparison of model predictions with experimental results at a strain rate of 8000/s.

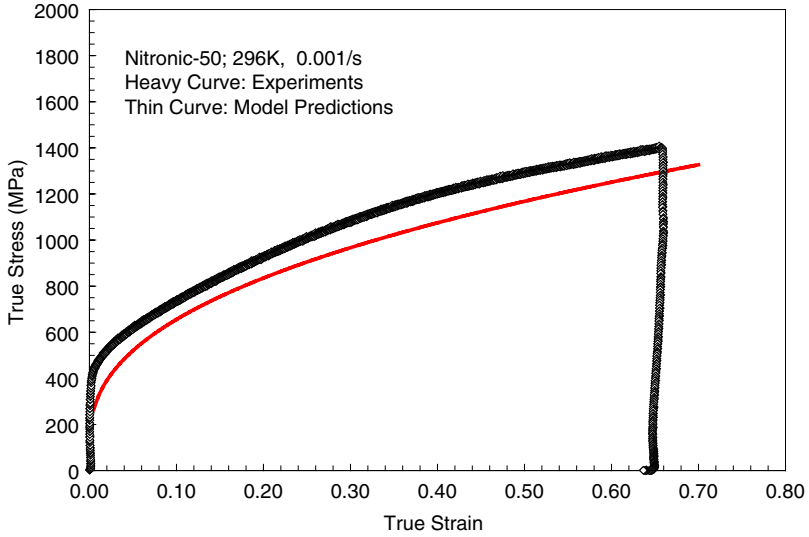

Fig. 14. Comparison of model predictions with experimental results at a strain rate of 0.001/s.

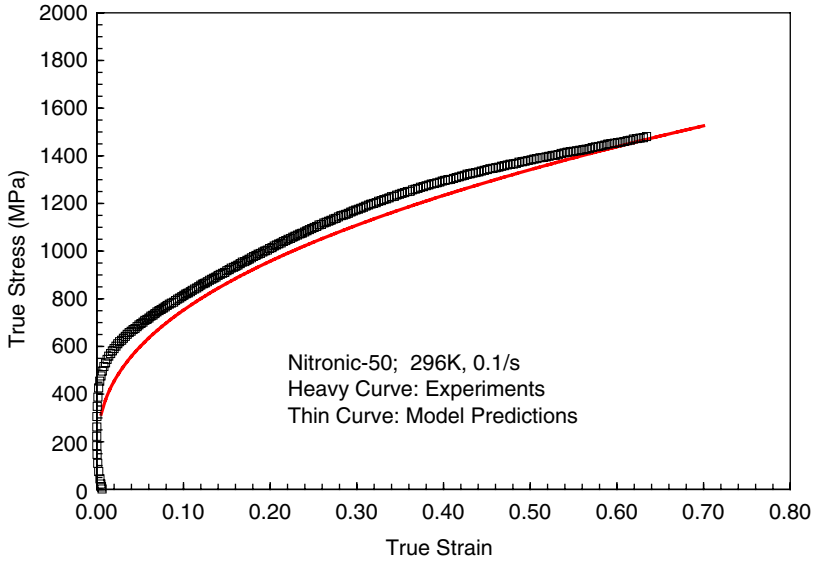

Fig. 15. Comparison of model predictions with experimental results at a strain rate of 0.1/s.

4. Conclusions

Uniaxial compression tests of cylindrical samples are performed to investigate the flow stress behavior of Nitronic-50 austenitic stainless steel. Strains exceeding 35% are achieved in these tests, over the range of strain rates from 0.001/s to about 8000/s, and at temperatures from 77 K to 1000 K. Several noteworthy conclusions are as follows:

1. Nitronic-50 stainless steel displays good ductility (strain $>$ 35%) at low temperatures and high strain rates, and, also greater ductility at higher temperatures.
2. Dynamic strain aging occurs in a temperature range from 400 K to 1000 K at lower strain rates, becoming less pronounced with the increasing strain. The maximum peak value of the stress in dynamic strain aging occurs at about a 700 K temperature for a 0.001/s strain rate.

3. The temperature has a greater effect on the flow stress of Nitronic-50 than does the strain rate.
4. Based on the experimental results, taking into account the viscous-drag effect, a physically based model is developed, which, in the absence of dynamic strain aging, has predictions that are in good agreement with the experimental results over a wide range of temperatures and strain rates.

References

Beukel, A.V.D., Kocks, U.F., 1982. The strain dependence of static and dynamic strain-aging. Acta Metall. 30, 1027–1034.

Brooks, J.A., Lippold, J.C., 1990. Selection of wrought austenitic stainless steels. ASM Handbook, vol. 6. ASM International, USA, pp. 457–469.

Chiem, C.Y., 1992. Material deformation at high strain rates. In: Meyers, M., Murr, L., Staudhammer, K. (Eds.), Shock-Wave and High-Strain-Rate Phenomena in Materials. Marcel Dekker, Inc., pp. 69–85.

Cho, Sang-Hyun, Yoo, Yeon-Chul, Jonas, J.J., 2000. Static and dynamic strain aging in 304 austenitic stainless steel at elevated temperature. J. Mater. Sci. Lett. 19, 2019–2022.

Conrad, H., 1970. The athermal component of the flow stress in crystalline solids. Mater. Sci. Eng. 6, 260–264.

Denhard, E.E., Espy, R.H., 1972. Austenitic stainless with unusual mechanical and corrosion properties. Met. Eng. Q. (November), 18–20.

Follansbee, P.S., Weertman, J., 1982. On the question of flow stress at high strain rates controlled by dislocation viscous flow. Mech. Mater. 1, 345–350.

Hecker, S.S., Stout, M.G., Staudhammer, K.P., Smith, J.L., 1982. Effect of strain state and strain rate on deformation-induced transformation in 304 stainless steel. 1. Magnetic measurements and mechanical behavior. Metall. Trans. A 13, 619–626.

Ishikawa, K., Tanimura, S., 1992. Strain rate sensitivity of flow stress at low temperatures in 304N stainless steel. Int. J. Plast. 8, 947–958.

Kapoor, R., Nemat-Nasser, S., 1998. Determination of temperature rise during high strain rate deformation. Mech. Mater. 27, 1–12.

Kocks, U.F., Argon, A.S., Ashby, M.F., 1975. Thermodynamics and kinetics of slip. Prog. Mater. Sci. 19, 1–271.

Kubin, L.P., Estrin, Y., Perrier, C., 1992. On static strain aging. Acta Metall. 40, 1037–1044.

Nakada, Y., Keh, A.S., 1970. Serrated flow in Ni–C alloys. Acta Metall. 18, 437–443.

Nemat-Nasser, S., 2004. Plasticity: A Treatise on Finite Deformation of Heterogeneous Inelastic Materials. Cambridge University Press.

Nemat-Nasser, S., Isaacs, J.B., 1996. Direct measurement of isothermal flow stress of metals at elevated temperatures and high strain rates with application to Ta and Ta–W alloys. Acta Mater. 45, 907–919.

Nemat-Nasser, S., Li, Y.L., 1998. Flow stress of fcc polycrystals with application to OFHC Cu. Acta Mater. 46, 565–577.

Nemat-Nasser, S., Isaacs, J.B., Starrett, J.E., 1991. Hopkinson techniques for dynamic recovery experiments. Proc. R. Soc. London 435 (A), 371–391.

Nemat-Nasser, S., Guo, W.G., Cheng, J.Y., 1999. Mechanical properties and deformation mechanisms of a commercially pure titanium. Acta Mater. 47, 3705–3721.

Nemat-Nasser, S., Guo, W.G., Kihl, D.P., 2001. Thermomechanical response of AL-6XN stainless steel over a wide range of strain rates and temperatures. J. Mech. Phys. Solids 49, 1823–1846.

Ono, K., 1968. Temperature dependence of dispersed barrier hardening. J. Appl. Phys. 39, 1803–1806.

Regazzoni, G., Kocks, U.F., Follansbee, P.S., 1987. Dislocation kinetics at high strain rates. Acta Metall. 35, 2865–2875.

Ritter, A.M., 1988. Sigma-phase formation in Nitronic-50 and Nitronic-50W stainless steels. J. Mater. Sci. 23, 3348–3356.

Ritter, A.M., Henry, M.F., 1985. Phase transformations during aging of a nitrogen-strengthened austenitic stainless steel. Metall. Trans. A 16A, 1759–1771.

Stout, M.G., Follansbee, P.S., 1986. Strain rate sensitivity, strain hardening, and yield behavior of 304L stainless steel. Trans. ASME, J. Eng. Mater. Tech. 108, 344–353.

Zerilli, F.J., Armstrong, R.W., 1992. The effect of dislocation drag on the stress–strain behavior of fcc metals. Acta Metall. Mater. 40, 1803–1808.